Deep Spectra P2E: AI-Driven Spectral ECG Reconstruction from PPG for Continuous Cardiovascular Monitoring

Shyamala Subramanian
Symbiosis Institute of Technology, Pune Campus, Symbiosis International (Deemed University), Pune, 412115, India | Department of Electronics and Telecommunication, SIES Graduate School of Technology, Navi Mumbai, India
shyamalamathi123@gmail.com (corresponding author)

Sashikala Mishra
Symbiosis Institute of Technology, Pune Campus, Symbiosis International (Deemed University), Pune, 412115, India
sashikala.mishra@sitpune.edu.in

Manoj Kumar
School of Computer Science, FEIS, University of Wollongong in Dubai, Dubai Knowledge Park, Dubai, United Arab Emirates
manojkumar@uowdubai.ac.ae

Ketan Kotecha
Symbiosis Institute of Technology, Pune Campus, Symbiosis International (Deemed University), Pune, 412115, India | Symbiosis Centre for Applied Artificial Intelligence (SCAAI), Symbiosis International (Deemed University) (SIU), Pune, 412115, India
director@sitpune.edu.in

Kailash Shaw
Department of Computer Science and Engineering (AI&ML), Vishwakarma Institute of Technology, Pune, 411037, Maharashtra, India
kailash.shaw@gmail.com

Received: 3 August 2025 | Revised: 8 September 2025 and 18 September 2025 | Accepted: 20 September 2025

 DOI: https://doi.org/10.48084/etasr.13805

ABSTRACT

The increasing prevalence of cardiovascular diseases demands affordable, accessible, and continuous cardiac monitoring solutions. Although an Electrocardiogram (ECG) is considered the clinical gold standard, long-term real-time monitoring of healthy individuals is limited. On the other hand, photoplethysmography is a simple and cost-effective technique, but it can be susceptible to noise and signal distortion. This study attempts to bridge the gap by proposing a novel framework for Photoplethysmogram (PPG) to ECG transformation, using spectral transformation methods such as Short-Time Fourier Transform (STFT), Discrete Cosine Transform (DCT), Wavelet Transform (WT), and Fast Fourier Transform (FFT). Deep learning models, namely Convolutional Neural Network (CNN), Convolutional Neural Network-Gated Recurrent Unit (CNN-GRU), and Convolutional Neural Network-Long Short-Term Memory (CNN-LSTM), were trained on the UCI Machine Learning Repository version of the MIMIC II dataset and PulseDB Vital datasets to reconstruct ECG from PPG, achieving a correlation coefficient of 0.9731. Validated on MIMIC III, robustness was confirmed with a correlation of 0.9639. The proposed framework leverages frequency-domain representations and lightweight, efficient deep learning models, making it well-suited for integration into real-time and resource-limited environments, such as

wearable health monitoring systems, and serves as a foundation for future non-invasive blood pressure estimation using only PPG input.

Keywords-Photoplethysmogram (PPG); Electrocardiogram (ECG); reconstruction; cardiovascular diseases; CNN-LSTM; CNN-GRU; CNN; BP estimation; mean absolute error; standard deviation

I. INTRODUCTION

Cardiovascular Diseases (CVDs) accounted for 32% of global deaths in 2019 [1] and remain a leading cause of death, driven by sedentary lifestyles, obesity, stress, and smoking, highlighting the need for continuous cardiovascular monitoring [2]. Electrocardiography (ECG) is the standard for diagnosing heart conditions. However, its cost and reliance on expert analysis limit long-term, daily use [3, 4]. Photoplethysmography (PPG), a non-invasive and low-cost optical method that enables heart monitoring via wearables [5-7]. Despite its convenience, PPG lacks detailed cardiac features and is prone to motion artifacts [6]. Previous studies have demonstrated a significant correlation between PPG and ECG signals, as the peripheral blood volume changes detected by PPG are directly influenced by the electrical activity of the heart captured in ECG records. Modified U-Net [8] and hybrid attention-based neural networks [9] have been designed to reconstruct ECG signals from PPG inputs, using the strong correlation between these modalities. Given the global burden of CVD, Machine Learning (ML) methods are explored to enable early detection and long-term monitoring [1]. DL models, such as CNNs and RNNs, enhance the accuracy of PPG-to-ECG (P2E) conversion and support integration into wearable technologies. This work improves P2E conversion using frequency-domain methods and DL. Key contributions include: (i) Reducing time-domain complexity via spectral representations while preserving physiological details, (ii) Comparing FFT, DCT, Wavelet, and STFT to find optimal frequency-domain transformation, (iii) Using CNN, CNN-GRU, and CNN-LSTM models to reconstruct ECG from spectral PPG, and (iv) Proposing a real-time, low-resource pipeline suitable for wearable devices. The reconstructed ECG can also support downstream tasks such as BP estimation. STFT-transformed signals improve BP estimation, eliminating the need for electrodes and enabling fully non-invasive pipelines. The proposed framework enhances monitoring efficiency and generalizes across datasets, including MIMIC III. Model generalizability is also tested on an independent dataset.

II. RELATED WORK

P2E mapping has emerged as a promising strategy for non-invasive cardiovascular monitoring. Approaches include generative models, signal reconstruction, and DL frameworks. GANs have been applied to model ECG signals with complex morphology [10, 11]. Recent works also explored diffusion-based synthesis [12, 13]. Early P2E models used linear techniques, such as regression and dictionary learning [14, 15]. Adaptive filters, PCA, and wavelet decomposition have also been applied [16, 17]. DL models, such as RNNs [18], LSTMs [10], autoencoders [19], and CNN-RNN hybrids [20], have shown improved ECG recovery. P2ERM [19] proposed a memory-based autoencoder for real-time calibration. More recent studies include attention-driven [21], subject-specific [22], and transformer-based models [23], enabling personalized and real-time health tracking. Many models still operate in the time domain, demanding high sample rates and computational resources. Despite training on large datasets, such as UCI-MIMIC II [18] and MIMIC III [10, 19], deployment in real-time settings may be limited. Additionally, static training splits and PPG variability reduce model generalization. Spectral approaches (FFT, DCT, Wavelet, STFT) offer compact, informative representations, improving efficiency and feature extraction for tasks like BP estimation, as they reduce dimensionality while preserving key cardiac features. This study addresses current limitations by developing a frequency-domain P2E model that enhances generalization and reduces computational complexity. The proposed model is validated across subjects and datasets for real-time application.

III. METHODOLOGY

This section outlines the approach for converting PPG into a frequency-transformed ECG, consisting of data preprocessing, frequency transformation, DL-based conversion, and performance evaluation. Figure 1 illustrates the overall workflow, which begins with raw PPG and ECG signals sourced from two datasets, namely, UCI-MIMIC II and PulseDB Vital. The signals are segmented, subjected to a Signal-to-Noise Ratio (SNR) threshold, and then transformed into the spectral domain using FFT, DCT, wavelet transforms, and STFT methods. A DL model is then trained to reconstruct the ECG data representation from the PPG data representation, and its performance is evaluated using the Pearson correlation coefficient. The trained model is finally tested on the test dataset, which consists of concatenated UCI-MIMIC II and Pulse DB Vital data, and further validated on a completely separate dataset, MIMIC III, to assess generalization.

A. Datasets

This study used three datasets, the UCI Machine Learning Repository MIMIC II, PulseDB Vital, and MIMIC III, for the signal conversion. These datasets, available through PhysioNet, include synchronized ABP, ECG, and PPG signals with a sampling frequency (f_s) of 125 Hz. The UCI dataset comprises 12,000 records of synchronized PPG and ECG signals [24]. The PulseDB Vital dataset includes similar data, with synchronized PPG, ECG, ABP, and cardiovascular parameters, providing reference SBP and DBP values [25]. The MIMIC III dataset was used for independent validation of the P2E conversion model, with data sampled at 125 Hz and segmented into 8-second windows, similar to the other datasets [26].

Table I summarizes the features and preprocessing details for the UCI-MIMIC II, PulseDB Vital, and MIMIC III datasets, including the sampling frequency, number of records before and after selection, and final records used for P2E conversion. UCI-MIMIC II and PulseDB Vital were subsampled (1 in 4) due to memory constraints, while MIMIC III was reserved for independent testing.

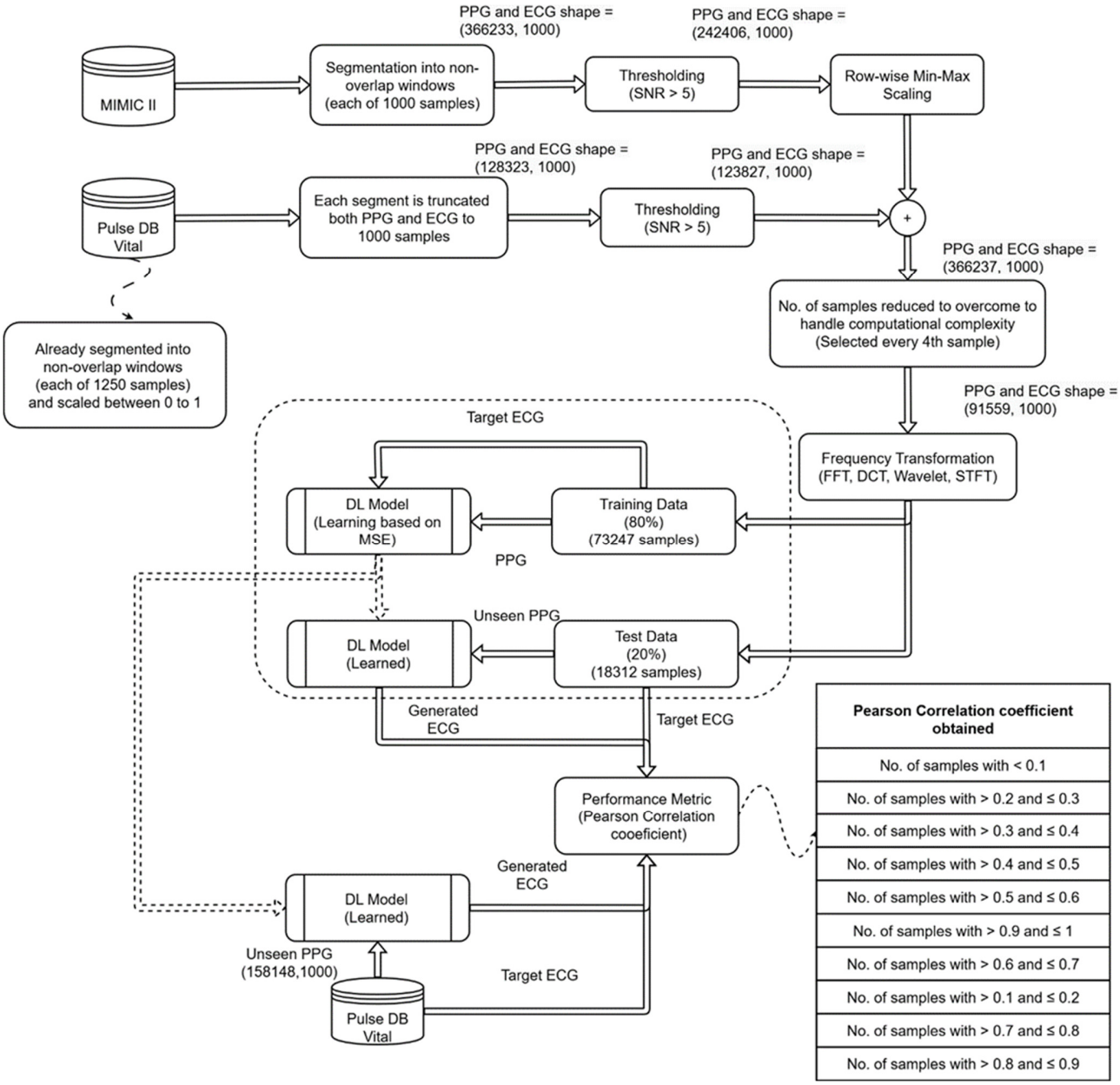

Fig. 1. Workflow for frequency-transformed PPG to ECG conversion.

TABLE I. SUMMARY OF DATASET CHARACTERISTICS, PREPROCESSING STEPS, AND RECORDS USED FOR P2E CONVERSION AND EVALUATION OF RECONSTRUCTED ECG SIGNALS

Dataset			**Original data**	**After SNR thresholding and truncating after 1000 samples (8 secs)**	**No. of records used in P2E conversion**	
UCI-MIMIC II	f_s = 125 Hz	No. of Subjects	Unknown	Unknown	After concatenating UCI-MIMIC II and Pulse DB Vital, No. of records = 3,66,233 ×1000	By selecting every 4th record, the total no. of records was reduced to 91,559×1000 to overcome memory issues.
		No. of Records	3,33,690 ×1000	2,42,406 × 1000		
Pulse DB Vital		No. of Subjects	247	242		
		No. of Records	1,28,323 ×1250	1,23,827 × 1000		
MIMIC III		No. of Subjects	109	108	1,49,896 ×1000	Used 1,49,896×1000 records to evaluate the P2E model generalization by comparing the original and reconstructed ECG
		No. of Records	158148 ×1250	1,49,896 × 1000		

B. Frequency Transformation

This aim was to convert PPG to ECG using frequency-domain transformations to address high sampling rates, reduce computational load, and enhance the model's ability to identify relevant features. DL models were trained to map frequency-transformed PPG signals to their ECG counterparts. Frequency transformations help extract informative signal components and improve computational efficiency. Four methods, FFT, DCT, STFT, and WT (Daubechies-db1), were selected for their ability to reveal signal associations between PPG and ECG.

1) Fast Fourier Transform (FFT)

The Discrete Fourier Transform (DFT) converts signals from the time to the frequency domain. It is best suited for stationary signals but lacks time-localized information, making it less ideal for non-stationary signals like PPG and ECG.

$$X(k) = \sum_{n=0}^{N-1} x(n) e^{-j2\pi \frac{kn}{N}} \quad (1)$$

where $X(k)$ represents the frequency-transformed signal and $x(n)$ is the time-domain signal. With 1000 samples per record, $N = 1000$. The transform is periodic and symmetric; hence, 500 coefficients are retained.

2) Discrete Cosine Transform (DCT)

DCT represents the signal as a sum of cosine functions. This transform is effective for energy compaction, concentrating energy in low-frequency components, where most PPG/ECG information resides. It simplifies representation and reduces redundancy, making it ideal for efficient P2E conversion.

$$X = \sum_{n=0}^{N-1} x(n) cos\left[\frac{\pi}{N}(n + 0.5)k\right] \quad (2)$$

3) Short-Time Fourier Transform (STFT)

STFT enables time-localized frequency analysis for non-stationary signals by segmenting them with overlapping windows and applying FFT to each segment. The STFT of a signal is given by:

$$X(m, k) = \sum_{n=0}^{N-1} x(n) w(n - m) e^{-j2\pi \frac{kn}{N}} \quad (3)$$

where $x(n)$ is the sequence, $w(n - m)$ is the sliding window function centered at time index m, $e^{-j2\pi \frac{kn}{N}}$ is the DFT kernel, and N is the number of points used. In this study, $nperseg = 64$ and $noverlap = 32$, providing a balance between time resolution and efficiency. The STFT output is represented as a spectrogram.

4) Wavelet Transforms

Wavelets allow multi-scale time-frequency analysis and are suitable for signals with varying frequency characteristics:

$$W(a, b) = \sum_t x(t) \psi^* \left(\frac{t-b}{a}\right) \quad (4)$$

where ψ is the wavelet function, a is the scale parameter, and b is the translation parameter. This formula represents the discrete version of the wavelet transform, where the signal is decomposed into wavelet coefficients at different scales and translations. This study used the Daubechies (db1) wavelet due to its ability to capture signal transitions. However, due to higher memory usage and limited gains over STFT, WT was computationally expensive and limited to 3000 samples. While frequency-domain transformation can also support downstream tasks, such as blood pressure estimation, this study focuses solely on reconstructing ECG signals from PPG data.

C. Deep Learning P2E Conversion Model

Deep learning-based architectures were used to transform PPG signals into ECG representations, facilitating advanced cardiovascular assessment and enabling potential future applications such as non-invasive BP estimation. Three models, CNN-GRU, CNN-LSTM, and CNN, were utilized to capture both spatial and temporal dependencies from PPG signals. Each transformation method (STFT, Wavelet (db1), DCT, and FFT) extracts distinct signal characteristics, allowing the models to effectively reconstruct spectral domain ECG from PPG inputs. The convolutional layers in these architectures extract local spatial features, while the LSTM and GRU components help capture long-range dependencies in the signal, enhancing temporal feature representation. CNN-GRU demonstrated superior performance in capturing temporal variations, particularly when using STFT-transformed inputs, as further detailed in the results section. Table II presents the architectural details of CNN, CNN_LSTM, and CNN_GRU models, highlighting their layer configurations, parameters, and structural differences used for feature extraction and sequence modeling. Each model learns a function f_θ that maps the PPG signal X_{PPG} to the corresponding ECG signal Y_{ECG} as:

$$Y_{ECG} = f_\theta(X_{PPG}) \quad (5)$$

where f_θ represents the DL model with trainable parameters θ. The convolutional layers extract local spatial features from the transformed PPG input $X_{PPG} \in \mathbb{R}^{h \times w \times c}$ using (6) for convolution operations.

$$Z^{(l)} = \sigma(W^{(l)} * X^{(l)} + b^{(l)}) \quad (6)$$

where $W^{(l)}$ and $b^{(l)}$ are weights and biases of the convolutional layer at depth l, $*$ is the convolution operation, and σ is the activation function (ReLU). To improve feature extraction and enhance model performance, additional components were incorporated into the convolutional layers of all models:

- Squeeze and Excitation (SE) Block: Dynamically standardizes channel-wise feature response to enhance feature representation.
- Residual Connections: Facilitates better information flow and mitigates the vanishing gradient problem.
- Layer normalization: Stabilizes activations, improving training convergence and generalization.
- Multiscale convolution: Employs filters of different sizes to capture both local and global patterns.
- Global Average Pooling (GAP): Reduces the number of parameters, preventing overfitting.
- Dropout in fully connected layers: Introduced to prevent overfitting.

The extracted features are passed through LSTM/GRU layers for temporal modeling, where both the hidden state h_t and cell state c_t evolve, as shown in (7) for LSTM:

$$c_t, h_t = LSTM(X_t, c_{t-1}, h_{t-1}) \quad (7)$$

Hidden state h_t evolves as shown in (8) for GRU:

$$h_t = GRU(X_t, h_{t-1}) \quad (8)$$

CNN-GRU with STFT outperformed other variants in modeling temporal dynamics. Models were trained using a two-stage strategy. First, 10-fold cross-validation over 10 epochs was performed using MSE loss. The effectiveness of the models was assessed using the Pearson correlation coefficient. The best model was retrained on the full dataset for 50 epochs with early stopping to improve generalization. This ensured full dataset utilization while preventing overfitting. The model was trained and validated on UCI-MIMIC II and PulseDB Vital datasets, and evaluated on unseen MIMIC III data. Results were categorized into bins based on correlation to quantify model performance. CNN-GRU with STFT yielded the highest accuracy.

While not explored in this work, the reconstructed ECG signals may support downstream tasks such as blood pressure estimation in future studies, offering potential for future applications such as non-invasive cardiovascular assessments, including blood pressure estimation. Enhanced design elements (SE blocks, residuals, multiscale filters) improve modeling across spectral inputs.

TABLE II. ARCHITECTURES OF CNN, CNN_LSTM, CNN_GRU

Model	Input shape	Convolutional layers	Temporal layer	Dense layers	Loss function/ Evaluation metrics	Optimizer and validation	Other features
CNN-GRU	STFT: (33, 33, 1), FFT: (500, 1), DCT: (300, 1), DB1: (1000,1)	C1: 64 filters (5, 5), C2: 64 filters (3, 3), ReLU, Max-Pooling, Dropout (0.3)	GRU (128 units)	Dense layer: 128, Output dense layer: STFT: 33*33, FFT: 500, DCT: 300, DB1: 1000	MSE (Mean Squared Error)/ Pearson correlation	Adam optimizer, 10-fold cross-validation for performance	Squeeze-and-Excitation (SE) block, Residual connections, Layer normalization, multi-scale convolution
CNN-LSTM	STFT: (33, 33, 1), FFT: (500, 1), DCT: (300, 1), DB1: (1000,1)	C1: 64 filters (5, 5), C2: 64 filters, ReLU, Max-Pooling, Dropout (0.3)	LSTM (128 units)			Adam optimizer, 10-fold cross-validation for performance	Squeeze-and-Excitation (SE) block, Residual connections, Layer normalization, multi-scale convolution
CNN	STFT: (33, 33, 1), FFT: (500, 1), DCT: (300, 1), DB1: (1000,1)	C1: 32 filters (5,5), C2: 64 filters (3,3), C3: 128 filters (3,3) ReLU, Max-Pooling, Dropout (0.2)	-	Dense layer: 128, Dense layer: 128, Output dense layer: STFT: 33*33, FFT: 500, DCT: 300, DB1: 1000		Adam optimizer, 10-fold cross-validation for performance	SE block, Residual connections, GAP, Layer normalization, Dropout in dense layer

IV. RESULTS AND DISCUSSION

The CNN-GRU, CNN-LSTM, and CNN models were trained and evaluated on the UCI-MIMIC II and PulseDB Vital datasets for spectral ECG reconstruction. Evaluation was conducted in two stages: (i) Within-dataset performance on UCI-MIMIC II and PulseDB Vital, (ii) Cross-dataset generalization on unseen MIMIC III. CNN-GRU obtained the best overall performance.

A. Evaluation on UCI-MIMIC II and PulseDB Vital Datasets

The proposed P2E approach was evaluated using an 80-20 train-test split. The models were tested across STFT, Wavelet (db1), DCT, and FFT transformations to assess their ability to extract ECG features from PPG. STFT outperformed other transformations, with CNN-GRU achieving the best results by capturing temporal dependencies. Wavelet (db1) performed slightly lower, with a minimal difference between CNN-GRU and CNN-LSTM. DCT slightly favored CNN-LSTM, and FFT showed moderate performance, highlighting the effectiveness of STFT. Figure 2 shows that STFT-CNN-GRU achieved the highest correlation. Several studies have explored P2E conversion using metrics such as Pearson correlation, Mean Absolute Error (MAE), and Root Mean Square Error (RMSE). In contrast to subject-specific models, the proposed CNN-GRU model generalizes across datasets without requiring explicit signal alignment. In addition to accuracy, computational complexity was also analyzed in terms of trainable parameters, GFLOPs, and inference time. Table III summarizes this comparison for the three models.

TABLE III. COMPUTATIONAL COMPLEXITY OF THE MODELS WITH STFT TRANSFORMED DATA

Model	Trainable parameters	GFLOPs (per sample)	Inference time
CNN	351,809	0.0108	5.76 ms
CNN-GRU	270,081	0.0137	11.05 ms
CNN-LSTM	294,401	0.0137	11.23 ms

Table IV presents a comparison with previous works. The proposed model achieved a correlation of 0.9647 with an MAE of 0.18 and an RMSE of 0.031, indicating strong reconstruction quality. Although BP estimation was not included, the reconstructed ECG signals are expected to support future non-invasive BP prediction tasks. Previous studies showed enhanced performance when using both PPG and ECG for BP estimation. Thus, the proposed framework may serve as a valuable preprocessing step, improving reliability in downstream clinical applications. Although the primary focus of this study is spectral ECG reconstruction from PPG, the high-fidelity outputs lay a strong foundation for future tasks such as non-invasive BP estimation, offering potential for continuous cardiovascular monitoring.

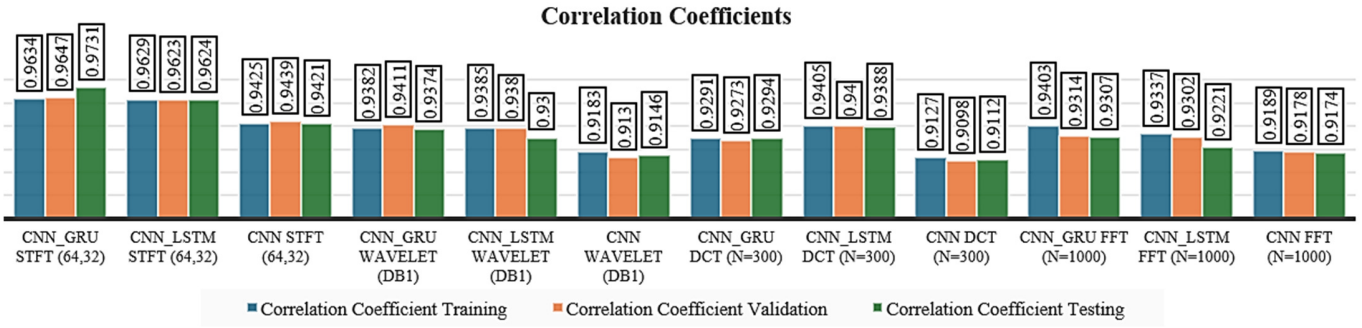

Fig. 2. Comparison of correlation coefficients across different models (CNN-GRU, CNN-LSTM, and CNN)

TABLE IV. COMPARISON WITH EXISTING STUDIES ON PPG-TO-ECG RECONSTRUCTION.

Ref.	CC	MAE	RMSE	Information
[9]	0.818	-	0.083	Developed a subject-specific deep learning model based on bidirectional LSTM for ECG reconstruction from PPG.
[17]	-	-	0.031	Proposed a hybrid attention-based model with Stochastic Gradient Descent for ECG reconstruction from PPG signals.
[20]	0.847	-	0.076	Model trained on a small, noisy dataset; demonstrated potential for continuous AF monitoring.
[21]	0.977	-	0.037	The proposed model does not require signal alignment; evaluated on a dataset of 500 records.
[22]	-	-	0.29	Introduced a transformer-based architecture, achieving an RMSE of 0.29 mV on the BIDMC database.
[27]	0.851	-	0.075	Demonstrated a group model setup with high correlation coefficients.
Proposed model	0.9647	0.18	0.031	Developed a CNN-GRU model for P2E signal reconstruction, validated on an unseen dataset (MIMIC III), and demonstrating strong generalization.

B. Generalization on the MIMIC III Dataset

The models were trained on the combined UCI-MIMIC II and PulseDB Vital datasets and tested on the unseen MIMIC III dataset to assess generalizability, with the results shown in Figure 3.

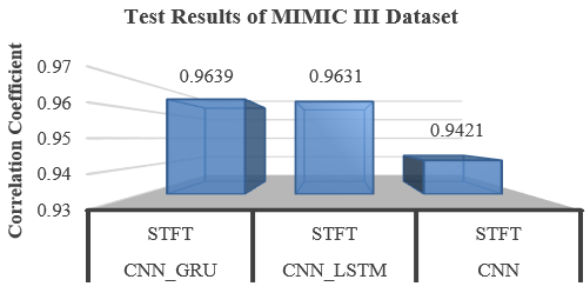

Fig. 3. Pearson correlation coefficient of three models (CNN_GRU, CNN_LSTM, CNN) on MIMIC III.

A total of 149,896 test samples were analyzed, with Pearson correlation coefficients grouped into ranges (Table V) and visualized in Figure 4. This demonstrates the model's ability to generalize without retraining or alignment. CNN-GRU reconstructed more than 78% of ECG samples with correlation above 0.9, outperforming CNN and CNN-LSTM. This confirms its robustness across patient conditions. The proposed CNN-GRU model, combined with frequency-domain inputs such as STFT, is designed for computational efficiency and low-latency processing, aligning well with real-time applications. By converting signals into compact frequency-domain representations, the model reduces data dimensionality and accelerates inference, supporting continuous monitoring. Training and validation on 8-second signal windows enable compatibility with real-time signal acquisition.

The use of GRU units, instead of more complex architectures like LSTM or transformers, helps minimize computational overhead while preserving temporal fidelity. Additionally, the model's strong generalization across unseen datasets, particularly MIMIC III, reinforces its robustness and adaptability, making it suitable for wearable or edge-based health monitoring systems. The results confirm high-fidelity signal recovery and generalization across datasets. The CNN-GRU model, in particular, exhibits strong generalization and robust performance, making it well-suited for practical deployment in diverse physiological settings.

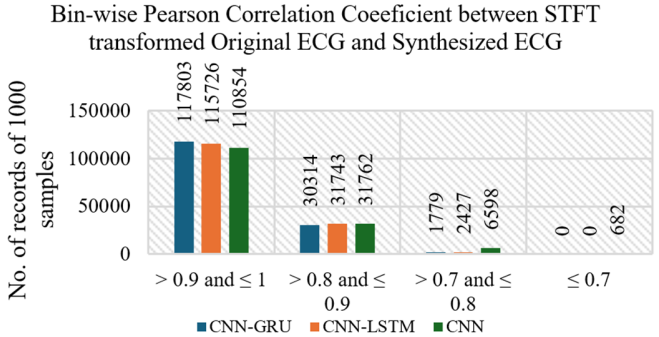

Fig. 4. Distribution of correlation coefficients for CNN-GRU, CNN-LSTM, and CNN models across different ranges on MIMIC III.

TABLE V. DISTRIBUTION OF MIMIC III SAMPLES ACROSS CORRELATION RANGES FOR CNN-GRU, CNN-LSTM, AND CNN MODELS

Correlation coefficient	CNN-GRU		CNN-LSTM		CNN	
	No. of samples	% of samples	No. of samples	% of samples	No. of samples	% of samples
> 0.9 and ≤ 1	117803	78.590	115726	77.204	110854	73.954
> 0.8 and ≤ 0.9	30314	20.223	31743	21.177	31762	21.189
> 0.7 and ≤ 0.8	1779	1.187	2427	1.619	6598	4.402
≤ 0.7	0	0.000	0	0.000	682	0.455

The key findings of this study can be summarized as:

- Optimal Transformation Selection: Among the transformations, STFT emerged as the most effective in preserving both temporal and frequency-based characteristics. It enabled the model to extract meaningful signal patterns for accurate ECG reconstruction and potential BP estimation.
- Model Performance: CNN-GRU demonstrated slightly better generalization than CNN-LSTM, particularly when trained on STFT-transformed data. This suggests that the gated recurrent mechanism in GRU effectively captures long-range dependencies while reducing computational demands, enhancing its real-time applicability.
- Robust Predictions: CNN-GRU exhibited strong and slightly better performance than CNN-LSTM on unseen data, demonstrating adaptability to different physiological signal variations. This confirms reliability in real-world ECG reconstruction and potential BP estimation.
- High Correlation Validation: The models achieved high Pearson correlation, particularly on MIMIC III, reinforcing the robustness of the approach. These results highlight the effectiveness of DL in analyzing physiological signals and support the feasibility of using frequency-domain approaches for non-invasive cardiovascular monitoring.

These results confirm that high-fidelity ECG reconstruction from PPG is feasible and scalable across datasets—offering a strong foundation for future non-invasive monitoring solutions.

V. CONCLUSION

This study presented a different approach to transform PPG signals into ECG representations using frequency-domain transformations and DL techniques, which showed a noticeable improvement compared to conventional time-domain methods. The key novelty is the introduction of a frequency-domain deep learning framework that reconstructs ECG from PPG, establishing the first step toward a hybrid, fully non-invasive, and wearable-compatible BP estimation system. Using FFT, DCT, Wavelet, and STFT, this framework optimizes feature extraction and reduces computation time, thus becoming suitable for real-time applications in cardiovascular monitoring. Using CNN, CNN-GRU, and CNN-LSTM models further improves the signal conversion process, allowing high-fidelity and reliable ECG synthesis from PPG data. Evaluation on multiple datasets, including UCI-MIMIC II, PulseDB Vital, and MIMIC III, validates the robustness and versatility of the proposed approach. The high quality of the reconstructed ECG signals suggests potential utility in future non-invasive BP prediction pipelines, highlighting the clinical relevance of this work.

Building on this foundation, future work will focus on leveraging the reconstructed ECG signals to improve blood pressure estimation by using both PPG and reconstructed ECG as complementary inputs. Given that ECG acquisition typically requires electrodes and is less practical for continuous monitoring, the proposed direction aims to rely solely on PPG signal capture. The corresponding STFT-transformed ECG will be generated using the current framework. These two spectrally transformed signals, PPG and reconstructed ECG, will be utilized to estimate systolic and diastolic blood pressure. It is anticipated that combining STFT-transformed PPG and ECG features will yield more accurate results than using PPG alone, while preserving a fully non-invasive, wearable-compatible architecture. Therefore, this study establishes the foundational step toward a hybrid blood pressure estimation system that is both computationally efficient and well-suited for real-world mobile health applications.

REFERENCES

[1] "Cardiovascular Diseases (CVD)," *World Health Organization*, https://www.who.int/news-room/fact-sheets/detail/cardiovascular-diseases-(cvds).

[2] "World Heart Report 2023: Full Report," *World Heart Federation*. https://world-heart-federation.org/resource/world-heart-report-2023/.

[3] Y. Sattar and L. Chhabra, "*Electrocardiogram,*" in *StatPearls*, Treasure Island, FL, USA: StatPearls Publishing, 2025.

[4] M. Tounsi, H. Ali, A. T. Azar, A. Al-Khayyat, and I. K. Ibraheem, "Comprehensive Learning Salp Swarm Algorithm with Ensemble Deep Learning-based ECG Signal Classification on Internet of Things Environment." *Engineering, Technology & Applied Science Research*, vol. 15, no. 1, pp. 19492–19500, Feb. 2025, https://doi.org/10.48084/etasr.8702.

[5] J. Allen, "Photoplethysmography and its application in clinical physiological measurement," *Physiological Measurement*, vol. 28, no. 3, Oct. 2007, Art. no. R1, https://doi.org/10.1088/0967-3334/28/3/R01.

[6] M. Elgendi *et al.*, "The use of photoplethysmography for assessing hypertension," *NPJ Digital Medicine*, vol. 2, no. 1, June 2019, Art. no. 60, https://doi.org/10.1038/s41746-019-0136-7.

[7] P. H. Charlton, P. A. Kyriacou, J. Mant, V. Marozas, P. Chowienczyk, and J. Alastruey, "Wearable Photoplethysmography for Cardiovascular Monitoring," *Proceedings of the IEEE*, vol. 110, no. 3, pp. 355–381, Mar. 2022, https://doi.org/10.1109/JPROC.2022.3149785.

[8] R. A. Pinto, H. S. De Oliveira, E. Souto, R. Giusti, and R. Veras, "Inferring ECG Waveforms from PPG Signals with a Modified U-Net Neural Network," *Sensors*, vol. 24, no. 18, Jan. 2024, Art. no. 6046, https://doi.org/10.3390/s24186046.

[9] Q. Tang *et al.*, "Robust Reconstruction of Electrocardiogram Using Photoplethysmography: A Subject-Based Model," *Frontiers in Physiology*, vol. 13, Apr. 2022, Art. no. 859763, https://doi.org/10.3389/fphys.2022.859763.

[10] L. Berger, M. Haberbusch, and F. Moscato, "Generative adversarial networks in electrocardiogram synthesis: Recent developments and challenges," *Artificial Intelligence in Medicine*, vol. 143, Sept. 2023, Art. no. 102632, https://doi.org/10.1016/j.artmed.2023.102632.

[11] T. Golany and K. Radinsky, "PGANs: Personalized Generative Adversarial Networks for ECG Synthesis to Improve Patient-Specific Deep ECG Classification," *Proceedings of the AAAI Conference on Artificial Intelligence*, vol. 33, no. 01, pp. 557–564, July 2019, https://doi.org/10.1609/aaai.v33i01.3301557.

[12] Y. Lin *et al.*, "Biomedically Informed ECG Synthesis: Customizing Cardiac Cycle Phases with Diffusion Model," in *2024 IEEE International Conference on Bioinformatics and Biomedicine (BIBM)*, Lisbon, Portugal, Sept. 2024, pp. 3505–3508, https://doi.org/10.1109/BIBM62325.2024.10821878.

[13] T. Du, J. Wang, R. Qu, and Z. Zhu, "DS4U-Net: A Diffusion Model-Based Approach to Multi-Lead ECG Signal Generation," in *2024 9th International Conference on Intelligent Computing and Signal Processing (ICSP)*, Apr. 2024, Xian, China, pp. 867–871, https://doi.org/10.1109/ICSP62122.2024.10743556.

[14] R. Banerjee, A. Sinha, A. D. Choudhury, and A. Visvanathan, "PhotoECG: Photoplethysmographyto estimate ECG parameters," in *2014 IEEE International Conference on Acoustics, Speech and Signal Processing (ICASSP)*, Feb. 2014, Florence, Italy, pp. 4404–4408, https://doi.org/10.1109/ICASSP.2014.6854434.

[15] Q. Zhu, X. Tian, C. W. Wong, and M. Wu, "Learning Your Heart Actions From Pulse: ECG Waveform Reconstruction From PPG," *IEEE Internet of Things Journal*, vol. 8, no. 23, pp. 16734–16748, Sept. 2021, https://doi.org/10.1109/JIOT.2021.3097946.

[16] X. Tian, Q. Zhu, Y. Li, and M. Wu, "Cross-Domain Joint Dictionary Learning for ECG Reconstruction from PPG," in *ICASSP 2020 - 2020 IEEE International Conference on Acoustics, Speech and Signal Processing (ICASSP)*, Feb. 2020, Barcelona, Spain, pp. 936–940, https://doi.org/10.1109/ICASSP40776.2020.9054242.

[17] A. Ezzat, O. A. Omer, U. S. Mohamed, and A. S. Mubarak, "ECG signal reconstruction from PPG using a hybrid attention-based deep learning network," *EURASIP Journal on Advances in Signal Processing*, vol. 2024, no. 1, Nov. 2024, Art. no. 95, https://doi.org/10.1186/s13634-024-01158-8.

[18] N. Murmu, R. Gupta, and K. Das Sharma, "Real-Time PPG-to-ECG Reconstruction Model With On-Device Recalibration Facility," *IEEE Transactions on Instrumentation and Measurement*, vol. 73, pp. 1–9, 2024, https://doi.org/10.1109/TIM.2024.3450120.

[19] V. Bijalwan, V. B. Semwal, G. Singh, and T. K. Mandal, "HDL-PSR: Modelling Spatio-Temporal Features Using Hybrid Deep Learning Approach for Post-Stroke Rehabilitation," *Neural Processing Letters*, vol. 55, no. 1, pp. 279–298, Feb. 2023, https://doi.org/10.1007/s11063-022-10744-6.

[20] K. Vo, M. El-Khamy, and Y. Choi, "PPG-to-ECG Signal Translation for Continuous Atrial Fibrillation Detection via Attention-based Deep State-Space Modeling," in *2024 46th Annual International Conference of the IEEE Engineering in Medicine and Biology Society (EMBC)*, Orlando, FL, USA, July 2024, pp. 1–7, https://doi.org/10.1109/EMBC53108.2024.10781630.

[21] Q. Tang, Z. Chen, R. Ward, C. Menon, and M. Elgendi, "PPG2ECGps: An End-to-End Subject-Specific Deep Neural Network Model for Electrocardiogram Reconstruction from Photoplethysmography Signals without Pulse Arrival Time Adjustments," *Bioengineering*, vol. 10, no. 6, June 2023, Art. no. 630, https://doi.org/10.3390/bioengineering10060630.

[22] E. Lan, "Performer: A Novel PPG-to-ECG Reconstruction Transformer for a Digital Biomarker of Cardiovascular Disease Detection," in *2023 IEEE/CVF Winter Conference on Applications of Computer Vision (WACV)*, Waikoloa, HI, USA, Jan. 2023, pp. 1990–1998, https://doi.org/10.1109/WACV56688.2023.00203.

[23] K. Dashdondov and M. H. Kim, "Mahalanobis Distance Based Multivariate Outlier Detection to Improve Performance of Hypertension Prediction," *Neural Processing Letters*, vol. 55, no. 1, pp. 265–277, Feb. 2023, https://doi.org/10.1007/s11063-021-10663-y.

[24] M. Saeed *et al.*, "Multiparameter Intelligent Monitoring in Intensive Care II: A public-access intensive care unit database*," *Critical Care Medicine*, vol. 39, no. 5, May 2011, Art. no. 952, https://doi.org/10.1097/CCM.0b013e31820a92c6.

[25] H. C. Lee, Y. Park, S. B. Yoon, S. M. Yang, D. Park, and C. W. Jung, "VitalDB, a high-fidelity multi-parameter vital signs database in surgical patients," *Scientific Data*, vol. 9, no. 1, June 2022, Art. no. 279, https://doi.org/10.1038/s41597-022-01411-5.

[26] A. E. W. Johnson *et al.*, "MIMIC-III, a freely accessible critical care database," *Scientific Data*, vol. 3, no. 1, May 2016, Art. no. 160035, https://doi.org/10.1038/sdata.2016.35.

[27] Y. Guo, Q. Tang, S. Li, and Z. Chen, "Reconstruction of Missing Electrocardiography Signals from Photoplethysmography Data Using Deep Neural Network," *Bioengineering*, vol. 11, no. 4, Apr. 2024, Art. no. 365, https://doi.org/10.3390/bioengineering11040365.